Dual Estimation Approach to Falling-Ball Viscometry Using Terminal and Transient Velocity Data from Video Tracking

Mahendra Kusuma Nugraha[1a], Ernawatil Gani[1b], Berton M. Siahaan[1c]

[1]*Department of Physics, Faculty of Mathematics and Natural Science, Sam Ratulangi University, Malalayang, Manado City 95115, Indonesia*

Email: [a)]mahendrakusuma@unsrat.ac.id, [b)]ernawatilgani@unsrat.ac.id, [c)]bertonsiahaan@unsrat.ac.id

Abstract

In this study, a motion-tracking analysis method was applied to a viscometry system to measure free-fall velocity and determine the viscosity of a fluid. Experiments were conducted by dropping a marble into a tube containing the test liquid with known density, then recording its free-fall motion with a digital camera at 30 frames per second and analysing the data with Tracker software. From the calculated terminal velocity analysis across two trials ($(7.46 \pm 0.01) \times 10^{-4}$ m/s and $(8.64 \pm 0.01) \times 10^{-4}$ m/s), the viscosity values obtained were 3.0 Pa·s and 2.59 Pa·s, respectively, which are well within the acceptable range. An alternative approach using exponential curve fitting to analyse the transient phase did not yield results as accurate or comparable to the previous, because the data showed a linear relationship between position and time. In two consecutive trials, the viscosity values calculated using this method are 2.81×10^{-2} Pa·s and 3.02×10^{-2} Pa·s. This condition was likely caused by the camera's limited frame rate, which was insufficient to capture the continuous, subtle changes in downward velocity during the first phase of free-fall motion, which occurred over a very short period. Therefore, in a basic, simple yet standard experimental setup, viscosity can be reliably calculated only by measuring the terminal velocity in accordance with Stokes' law.

Keywords: viscometry; free-fall motion; terminal velocity; transient phase

INTRODUCTION

Object or motion tracking is a technique used to identify and determine the spatial position of a moving object over a specific time interval, utilising a camera or digital image as the data source. Advances in camera hardware technology and image processing algorithms enable continuous tracking across individual frames, allowing the object's trajectory to be measured with a high degree of accuracy (Karl *et al.*, 2018; Kadam, Fang and Zou, 2024). Essentially, this process begins with determining the object's initial position, followed by tracking its positional changes within the chosen coordinate throughout the video. The analysis is performed by splitting the footage into a series of 2-D frames (frame-by-frame), where the positional coordinates of the objects in each frame are extracted to form a position-time function. This function can then be mathematically derived to provide velocity and acceleration information (Karl *et al.*, 2018; Chen *et al.*, 2021). In practice, three-dimensional spatial data recorded by cameras is often represented as 2D images, requiring careful calibration procedures and parallax correction to ensure that the measured data approximates actual physical conditions (Abboud and Elbir, 2024; Kadam, Fang and Zou, 2024).

Modern tracking algorithms—both motion-based and appearance-based—are designed to maintain tracking accuracy despite variations in lighting, occlusion, and object rotation (Karl *et al.*, 2018; Kadam, Fang and Zou, 2024). The applications of motion/video tracking are varied, ranging from security monitoring and autonomous vehicle technology to augmented reality, medical imaging, and human-computer interaction. In the teaching of physics, this technique has proven to be a reliable method for obtaining kinematic parameters with high accuracy (Karl *et al.*, 2018; Akhlis *et al.*, 2020; Kadam, Fang and Zou, 2024). Its main advantage is the ability of software like Tracker to automatically record position, velocity, and acceleration with high temporal resolution, thereby reducing the errors caused by human measurement and saving raw data for later analysis (Akhlis *et al.*, 2020; Abboud and Elbir, 2024). Motion tracking and related approaches have been widely used as measurement techniques across multiple fields, including education (Chernetckiy *et al.*, 2021; Reuter and Schindler, 2023), medicine (Ganni *et al.*, 2018, 2020; Scott *et al.*, 2022) and computer technology (Liu and Xie, 2024).

Falling-ball viscometry has become one of the main subjects in laboratory-based physics education at the higher education level, alongside other types of simple experiments in mechanics, optics, and thermodynamics. This study utilised Tracker, a video analysis and modelling tool, in a falling-ball viscometry experiment, a method for measuring fluid viscosity by observing the free-falling, downward motion of a ball in a liquid medium (Akhlis *et al.*, 2020; Syifa, 2022). The advantage of this approach lies in the application of two viscosity estimators obtained from the same video data set: (i) an estimate based on the ball's terminal velocity, and (ii) an estimate from the transient phase through exponential curve fitting of the velocity versus time data. This dual-estimator strategy is a novel feature of the study because it allows internal cross-validation between calculation results, thereby increasing the accuracy and reliability of the measurements (Brizard *et al.*, 2005; Tang, 2016; Syifa, 2022; Pan *et al.*, 2025).

This method enables the simultaneous observation of the transient and terminal behaviour of the ball. This minimises errors due to the limitations of manual measurements and opens up opportunities for further studies on deviations from the ideal Stokes' law model. For example, due to wall effects, added mass, or changes in flow regime (Brizard *et al.*, 2005; Ballereau, Truong and Matias, 2016; Tang, 2016). Therefore, this study aims to confirm that the Tracker-based video tracking method not only provides more precise and informative experimental results than conventional methods, but is also more efficient in data collection and more reproducible under various conditions (Syifa, 2022; Abboud and Elbir, 2024; Pan *et al.*, 2025). Ultimately, this method offers a new analytical approach to falling-ball viscometry, aiming to gain a new perspective on how Stokes's law operates in ideal conditions, accounting for all physical constraints. By combining straightforward analytical and computational techniques (such as Tracker), the measurements are also expected to become increasingly accurate.

METHODS

This experiment employed a video-based analysis of falling-ball viscometry to determine the viscosity coefficient of a specific fluid. The procedure involves recording the movement of a glass marble as it freely descends within a column of liquid in a container, then analysing the video using Tracker software to determine the terminal velocity and transient motion parameters. The experimental apparatus consisted of a transparent cylindrical tube $(40 \pm 0.05) \times 10^{-2}$ m in height. Its inner diameter measures approximately $(6.6 \pm 0.05) \times 10^{-2}$ m, which is at least three times that of the test sphere to minimise wall effects. All length measurements were conducted using a standard-grade ruler with an uncertainty of 0.05×10^{-2} m. The tube was filled with a liquid soap of unknown viscosity. The fluid's density was calculated to be 972.2 kg/m³. The marble, made of glass, has a precisely measured diameter of 1.562×10^{-3} m and a mass of 5.3×10^{-3} kg. The density of the marble is approximately 2656 kg/m³, calculated by dividing its mass by its volume.

A tripod-mounted smartphone (Sharp AQUOS® Sense 4+, 8/128GB, 12 MP) capable of recording 1080p resolution and 30 frames per second (fps) captured the motion, as depicted in **FIGURE 1**. The scale embedded on the tube served as a spatial calibration marker, and adequate lighting was used to minimise motion blur and enhance clarity in the video. Before the trial, the fluid column was adjusted to the desired height and checked for the presence of air bubbles. The camera was positioned perpendicular to the motion plane to reduce perspective errors. The test sphere was carefully dropped from the top of the fluid surface without giving it horizontal velocity. Recording started before release and continued until the sphere reached the bottom of the tube. Each condition was repeated twice to ensure the accuracy of the measurement.

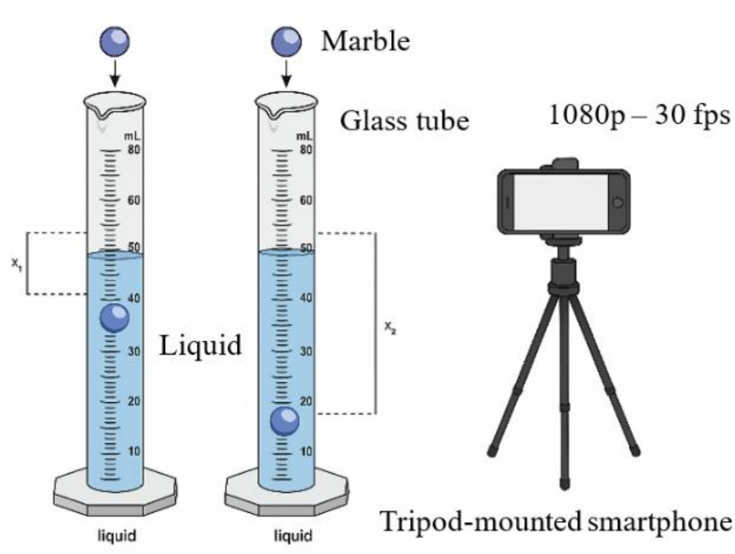

FIGURE 1. The schematic of the viscometry system.

The video recordings were then imported into Tracker (Open Source Physics). Spatial calibration was performed using the the built-in ruler feature, and a coordinate system was thereafter established with the negative y-axis pointing downwards in the direction of gravity. The track feature was used to locate and track the center location of the sphere in each frame. Position–time data were then analysed to determine instantaneous velocities along the drop. Viscosity was evaluated using two independent approaches. In the first step, terminal velocity was determined from the plateau region of the velocity–time graph and then substituted into Stokes' law to estimate viscosity. Stokes' drag with low Reynolds number is given by:

$$F_d = 6\pi\eta r v_t = (\rho_s - \rho_f) g \frac{4}{3}\pi r^3 \qquad (1)$$

where ρ_s and ρ_f are the marble and fluid density, respectively. Force balance at steady state:

$$v_t = \frac{2}{9} \times \frac{r^2(\rho_s - \rho_f)g}{\eta} \qquad (2)$$

Viscosity from terminal velocity:

$$\eta = \frac{2}{9} \times \frac{r^2(\rho_s - \rho_f)g}{v_t} \qquad (3)$$

which are the canonical Stokes formulas for settling spheres. The time constant without added mass correction can be derived as:

$$\tau = \frac{1}{\left(\frac{9}{2}\right)\frac{\eta}{\rho_s r^2}} = \frac{2}{9}\frac{\rho_s r^2}{\eta} \qquad (4)$$

The formula above assumes only Stokes drag and the sphere's mass. In reality, the effective inertia also includes the added mass of an accelerating fluid. The fluid entrained by an accelerating sphere acts like extra mass equal to half the displaced fluid's mass. The added mass correction becomes important when fluid density is not negligible compared to the sphere's density or when the time constant is short, such as during rapid transients. Therefore, the time constant formula with added mass correction is given by:

$$m_{eff} = \rho_s V + \frac{1}{2}\rho_f V \quad (5)$$

$$m_{eff} = \frac{4}{3}\pi r^3(\rho_s + \frac{1}{2}\rho_f) \quad (6)$$

$$\tau = \frac{m_{eff}}{6\pi\eta r} \quad (7)$$

The next step is to compute the particle Reynolds number using the characteristic terminal velocity to check Stokes validity ($Re \leq 1$), which indicates that the object moves in a strictly laminar fashion with negligible effect of turbulence:

$$Re = \frac{\rho_f v_t (2r)}{\eta} = \frac{2\rho_f r v t}{\eta} \quad (8)$$

Thus, based on the above explanation, the terminal velocity is reached when the object no longer experiences a change in speed, because the two mutually cancelling forces are gravity and the drag force exerted by the fluid through which the object passes. In a velocity-versus-time plot, the graph flattens into a horizontal plateau as the object approaches terminal velocity. In the case of the transient solution, the ODE is linear; therefore, with the general initial condition, the solution is:

$$v(t) = v_t + (v_0 - v_t)e^{-\frac{t}{\tau}} \quad (9)$$

$$y(t) = y_0 + v_t t - v_t \tau(1 - e^{-\frac{t}{\tau}}) \quad (10)$$

Thus, transient-derived η must use the corrected τ formula (or else it will be biased). The added mass for a sphere is approximately equal to half the displaced fluid mass. These two estimates were compared for cross-validation, with discrepancies examined in light of possible systematic errors such as wall effects, calibration inaccuracies, or deviations from laminar flow conditions. By using Tracker, the fitted time constant can be obtained automatically. The steps are to import the clip, calibrate the spatial scale using a ruler in the frame, set the coordinate axes, and run the auto-tracker to extract the position of the sphere in every frame. Next, the position–time data were modelled using the transient motion equation to yield the terminal velocity and derive the fitted time constant. The viscosity was computed independently, both from the terminal velocity (Stokes' law) and the fitted time constant with added mass correction for cross-validation.

RESULTS AND DISCUSSION

This section presents the results of observations and analysis of a glass marble's free-fall motion inside a tube filled with liquid soap of unknown viscosity. The marble was released precisely above the fluid surface to minimise the influence of initial velocity, ensuring that the observed motion accurately reflects the drag force exerted by the fluid. The distance travelled by the marble from the release point to the bottom of the tube was measured at $(21 \pm 0.01) \times 10^{-2}$ m. The average time taken was calculated from two consecutive trials, which lasted 2.73 s and 2.43 s. Environmental conditions during the experiment remained relatively stable, with minimal disturbance from external vibrations. The room temperature was measured to be between 29°C and 30°C.

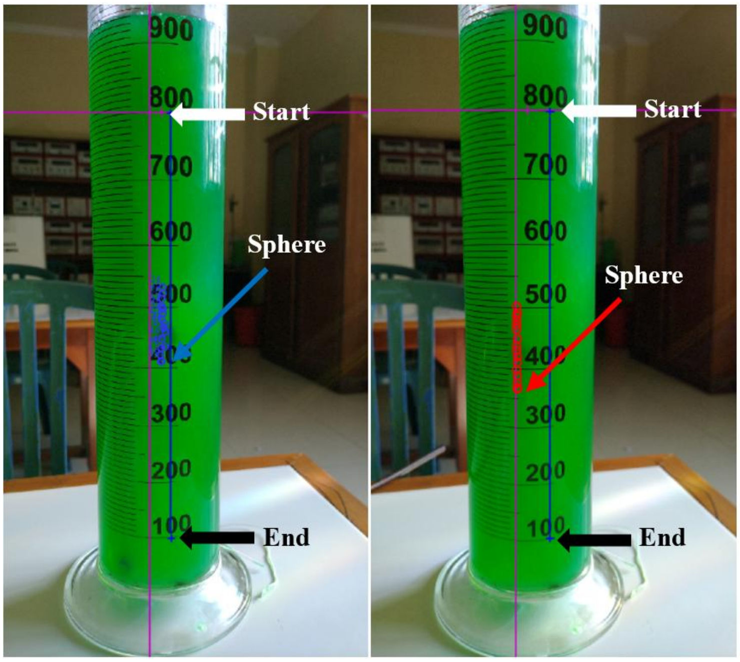

FIGURE 2. Free-fall motion tracking using the Tracker software.

FIGURE 2. shows a screenshot from the Tracker application during free-fall motion analysis. The position of the marble during tracking is indicated with trailing red and blue dots on the screen. The start and end points of the trajectory are clearly marked with a white and a black arrow, respectively. The color of the fluid did limit visual clarity; however, the test object remains easily identifiable, preventing ambiguity in position marking. The spatial calibration process involves adding a measuring rod installed parallel to the marble's movement path (thin blue line). This calibration aims to establish an accurate length scale and enhance the software's position detection accuracy. Additionally, the coordinate system on the screen—marked with a purple crossline—is aligned precisely parallel to the object's release point. This step is essential to ensure that the tracking data aligns with the reference frame used in subsequent quantitative analysis. Next, the mapped trajectory results are visualised in the form of a graph showing the relationship between the position of the marble on the Y-axis and the time taken at each observation point, as depicted in **FIGURE 3.a** and **3.b.**

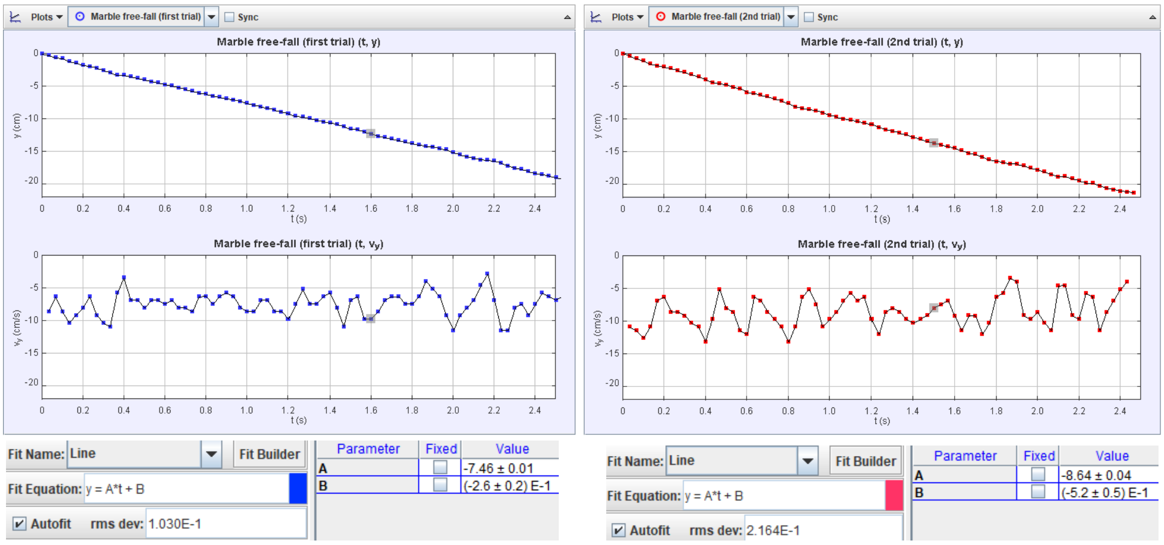

(a) **(b)**

FIGURE 3. (a) Position-time (top) and velocity-time (bottom) graph of the object in the first trial; and (b) in the second trial.

In general, the position data trend shows a linear trend over time, indicating that the marble's fall motion occurs with acceleration over a very short time and distance before reaching terminal velocity. Negative values on the graph indicate a consistent movement of the marble towards the negative side of the Y-axis, in accordance with the previously established coordinate system orientation. Additionally, a mapping of the magnitude of the object's velocity at each time interval is also provided. From this curve, small fluctuations in the velocity data, which are random in nature, can be observed; however, it is believed that they do not significantly affect the overall trend of the object's motion. The implementation of the linear fit feature in the Tracker application enables simple linear regression analysis, which then produces an estimate of the terminal velocity value as $(7.46 \pm 0.01) \times 10^{-4}$ m/s. In the regression equation, the gradient constant (parameter A) represents the slope of the curve. It is also interpreted as the magnitude of the terminal velocity reached by the object within the fluid medium during free-fall motion.

Applying the same procedure in the second experiment yielded results consistent with previous observations. As shown in **FIGURE 3.b**, the graph of the marble's position versus time again displays a linear pattern, reinforcing that the motion of falling in a fluid medium occurs at a steady rate, with minimal deviations from a simple linear model. This consistency also confirms the reliability of the tracking method used and shows that external disturbances were minimal under the experimental conditions. From the linear regression analysis of the second experiment, the terminal velocity was recorded as $(8.64 \pm 0.01) \times 10^{-4}$ m/s. The slight difference in terminal velocity values between the first and second experiments suggests that the experimental uncertainty is small and that the method's reliability is high.

The subsequent phase, derived from data collected from two experiments, entailed various mathematical computations to ascertain the fluid's viscosity, effective mass, and time constant up to the Reynolds number. These parameters—as presented below—will subsequently be employed for comparative analysis and validation against findings obtained via the transient fit method, with particular emphasis on the time constant and fluid viscosity.

The data in **TABLE 1**. show a slight difference in viscosity values between the first and second trial, mainly due to measurement precision and minor environmental variations rather than significant physical differences. The effective mass correction was applied to account for the fluid surrounding the accelerating sphere. Based on the values in **TABLE 2.**, the calculated Reynolds number ($\mathrm{R_e} < 1$) confirms that the object's motion occurs within the laminar regime and is primarily influenced by viscous forces. Therefore, it can be concluded that Stokes' drag law is valid under the current experimental conditions.

TABLE 1. The calculated viscosity and effective mass.

No.	Viscosity (η_{v_t})	Effective mass (m_{eff})
1	3.00 Pa · s	6.27×10^{-3} kg
2	2.59 Pa · s	

TABLE 2. Time constant and Reynolds number from terminal velocity.

No.	Time constant (τ_{v_t})	Reynolds number (R_e)
1	1.42×10^{-2} s	0.377
2	1.64×10^{-2} s	0.506

The subsequent phase of analysis in this experiment involves the application of an exponential fitting function to ascertain the transient time constant (τ). The transient time constant characterizes the rapidity with which an object attains its terminal velocity during free fall within a viscous medium. Nonetheless, the graphical data presented in **FIGURE 3**. exhibit predominantly a linear relationship between the object's position and time. However, the plot results can still be examined by fitting an exponential function to the determined linear curve. The built-in exponential function available within the Tracker application is provided as follows:

$$y = Ae^{Bt} + C \tag{11}$$

The appropriate formula applicable to transient velocity (assuming the absence of initial velocity) is as follows:

$$v(t) = v_t - v_t e^{-\frac{t}{\tau}} \tag{12}$$

Equation (12) can be modified to mathematically correspond with Equation (11), resulting in $A = -v_t$, $B = -1/\tau$ and $C = v_t$. The exponential fitting method conducted using Tracker indicates that the B coefficient values for both experiments are $6.6 \times 10^{-1}\ \mathrm{s}^{-1}$ and $7.1 \times 10^{-1}\ \mathrm{s}^{-1}$. Similar to the preceding approach, the viscosity value of the liquid can also be determined by reformulating equation (7) into the subsequent form:

$$\eta_{fit} = \frac{m_{eff}}{6\pi\tau_{fit} r} \tag{13}$$

Therefore, the time constant (τ_{fit}) derived from the exponential fitting, along with the calculated viscosity values of the liquid (η_{fit}), are presented jointly in the following table:

TABLE 3. Time constant and viscosity values from the transient fit.

No.	Time constant (τ_{fit})	Viscosity (η_{fit})
1	1.51 s	$2{,}81 \times 10^{-2}$ Pa · s
2	1.48 s	3.02×10^{-2} Pa · s

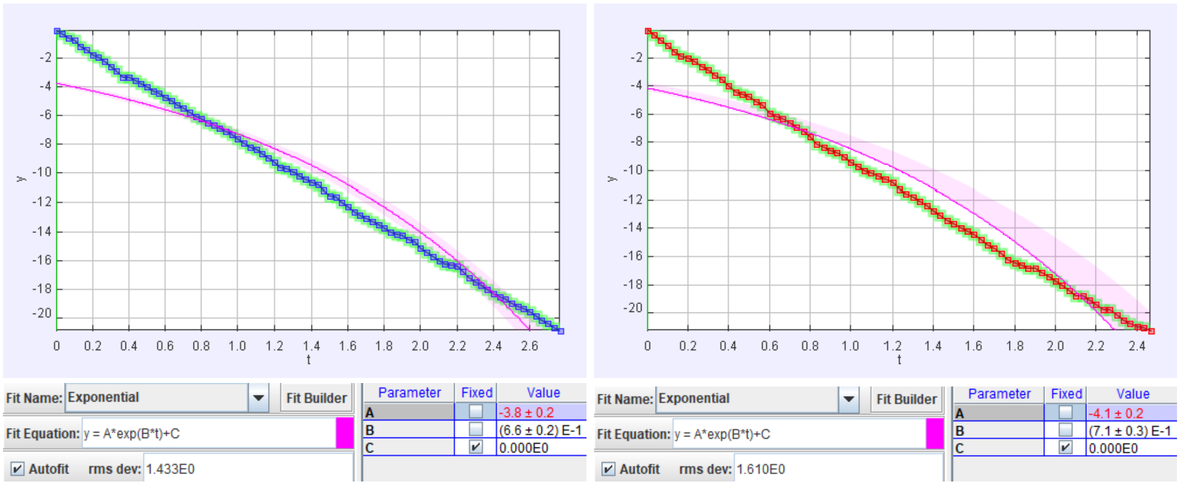

FIGURE 4. The linear interpretation for both of the trials is unsuitable for exponential fitting.

FIGURE 4. provides an overview of the exponential fitting methodology applied to the linear graph derived from two experiments. The results of these calculations also yield viscosity values for the fluid that differ markedly from those obtained via the preceding method (conventional approach).

This observation indicates that an exponential fit may not be suitable, as it could yield unreliable parameters. The findings suggest that the sphere attains its terminal velocity almost instantaneously after release, with no evident transient phase typically indicated by an exponential increase in velocity. In addition, wall effects are also believed to affect the obtained value, considering the ratio between the diameter of the marbles and the diameter of the tube (d/D) is only about three times. Therefore, further corrections may be needed to mitigate this condition.

The large fitted τ value does not mean a genuinely slow transient response; instead, it stems from the linearity of the velocity–time data. This indicates that the acceleration phase happened faster than the camera's temporal resolution could record, leading the exponential model to produce an unrealistically large time constant. This phenomenon is likely attributable to the limited frame rate of the recording device, which was insufficient to capture the brief acceleration period of the sphere. Consequently, although the analytical software offers an exponential fitting option, the data principally reflect only the terminal velocity regime.

CONCLUSION

Therefore, the analysis of fluid viscosity within this experiment can exclusively be performed employing the linearity method of terminal velocity based on Stokes' law. The terminal velocities of a falling marble in the fluid for the two experiments are recorded as $(7.46 \pm 0.01) \times 10^{-4}$ m/s and $(8.64 \pm 0.01) \times 10^{-4}$ m/s, respectively. A discrepancy exists between the viscosity values obtained from the first experiment (3.00 Pa·s) and the second (2.59 Pa·s), which is attributed solely to measurement errors rather than any significant physical factors. Nonetheless, these values remain within a certain range of the reference value, with potential deviations attributable to wall effects, calibration inaccuracies of the scale, or inhomogeneities in the release of the ball. Nevertheless, applying the transient fit method resulted in a viscosity value that deviated substantially from the terminal-based estimate, producing approximately 2.8×10^{-2} Pa·s and 3.02×10^{-2} Pa·s. This large discrepancy is due to the poorly resolved transient regime in the recorded data.

Several factors are believed to contribute to this situation, including the camera's inability to accurately capture the falling motion of the marbles. Although the limited frame rate restricts experimental transient analysis, theoretical calculations of τ may still be incorporated to enhance the discussion. This also underscores a significant point: measurements based on video tracking are highly contingent upon the temporal resolution of the equipment employed. For future research, the utilisation of high-speed cameras (≥ 240 fps) or selecting parameters for the ball and fluid that yield a larger τ could facilitate a more comprehensive transient analysis. A greater number of trials is also ensured to help improve the precision and accuracy of the calculation. Note that, under the current experimental condition, this work can only provide accurate viscosity measurements through terminal velocity analysis. In a more advanced setup of falling-ball viscometry, the transient-phase analysis is highly recommended as the primary method for determining the viscosity of a liquid due to its high level of accuracy.

ACKNOWLEDGEMENTS

We gratefully acknowledge the support of the staff at the Department of Physics, Faculty of Mathematics and Natural Sciences, Sam Ratulangi University. In particular, the assistance provided by the Modern Physics Laboratory team was essential to the success of this study.

REFERENCES

Abboud, K. and Elbir, B. (2024) "Calculating the Dynamic Viscosity of a Fluid using Image Processing of a Falling Ball," *Journal of Emerging Investigators* [Preprint]. Available at: https://doi.org/10.59720/23-198.

Akhlis, I. *et al.* (2020) "The Determination of Fluid Viscosity using Tracker-Assisted Falling Ball Viscosimeter," *Journal of Physics: Conference Series*. Institute of Physics Publishing. Available at: https://doi.org/10.1088/1742-6596/1567/4/042102.

Ballereau, P., Truong, D. and Matias, A. (2016) "Absolute Falling Ball Viscometer, Adapted to the Low Viscosities of Liquids," *International Journal of Metrology and Quality Engineering*, 7(3). Available at: https://doi.org/10.1051/ijmqe/2016015.

Brizard, M. *et al.* (2005) "Design of a High Precision Falling-Ball Viscometer," *Review of Scientific Instruments*, 76(2). Available at: https://doi.org/10.1063/1.1851471.

Chen, Z. *et al.* (2021) "Validity and Reliability of a Phone App and Stopwatch for the Measurement of 505 Change of Direction Performance: A Test-Retest Study Design," *Frontiers in Physiology*, 12. Available at: https://doi.org/10.3389/fphys.2021.743800.

Chernetckiy, I. *et al.* (2021) *The Application of Tracker Video Analysis for Distance Learning of Physics*. Available at: www.stemua.science.

Ganni, S. *et al.* (2018) "A software-based tool for video motion tracking in the surgical skills assessment landscape," *Surgical Endoscopy*, 32(6), pp. 2994–2999. Available at: https://doi.org/10.1007/s00464-018-6023-5.

Ganni, S. *et al.* (2020) "Validation of Motion Tracking Software for Evaluation of Surgical Performance in Laparoscopic Cholecystectomy," *Journal of Medical Systems*, 44(3). Available at: https://doi.org/10.1007/s10916-020-1525-9.

Kadam, P., Fang, G. and Zou, J.J. (2024) "Object Tracking Using Computer Vision: A Review," *Computers*. Multidisciplinary Digital Publishing Institute (MDPI). Available at: https://doi.org/10.3390/computers13060136.

Karl, J.M. *et al.* (2018) "Frame by Frame Video Analysis of Idiosyncratic Reach-to-Grasp Movements in Humans," *Journal of Visualized Experiments*, 2018(131). Available at: https://doi.org/10.3791/56733.

Liu, C. and Xie, Y. (2024) "Innovative Application of Computer Vision and Motion Tracking Technology in Sports Training," *EAI Endorsed Transactions on Pervasive Health and Technology*, 10. Available at: https://doi.org/10.4108/eetpht.10.5763.

Pan, Z. *et al.* (2025) "Precise Real-Time Measurement of Liquid Viscosity Using Digital Video Data," *Advanced Intelligent Systems* [Preprint]. Available at: https://doi.org/10.1002/aisy.202500297.

Reuter, A.S. and Schindler, M. (2023) "Motion Capture Systems and Their Use in Educational Research: Insights from a Systematic Literature Review," *Education Sciences*. MDPI. Available at: https://doi.org/10.3390/educsci13020167.

Scott, B. *et al.* (2022) "Healthcare applications of single camera markerless motion capture: a scoping review," *PeerJ*. PeerJ Inc. Available at: https://doi.org/10.7717/peerj.13517.

Syifa, N.H. (2022) "Determination oF Terminal Velocity And Fluid Viscosity using Falling Ball Viscometer with Video Tracker Application," *Jurnal Pendidikan Fisika*, 10(2), pp. 75–81. Available at: http://journal.uin-alauddin.ac.id/indeks.php/PendidikanFisika.

Tang, J.X. (2016) "Measurements of Fluid Viscosity using a Miniature Ball Drop Device," *Review of Scientific Instruments*, 87(5). Available at: https://doi.org/10.1063/1.4948314.